Advances in Aircraft and Spacecraft Science, *Vol. 5, No. 2 (2018) 277-294*
DOI: https://doi.org/10.12989/aas.2018.5.2.277

Comparison of mass operator methods considering test uncertainties

K. R. Olympio*[1], F. Blender[3], M. Holz[1], A. Kommer[1] and R. Vetter[2]

[1]Structural Engineering Dept., Airbus DS GmbH, Claude-Dornier Strasse, 88090 Immenstaad, Germany
[2]Mechanical AIT Dept., Airbus DS GmbH, Claude-Dornier Strasse, 88090 Immenstaad, Germany
[3]Mechanical Systems Germany Dept., Airbus DS GmbH, Claude-Dornier Strasse, 88090 Immenstaad, Germany

(Received December 18, 2016, Revised September 9, 2017, Accepted September 30, 2017)

Abstract. In the space industry, structures undergo several vibration and acoustic tests in order to verify their design and give confidence that they will survive the launch and other critical in-orbit dynamic scenarios. At component level, vibration tests are conducted with the aim to reach local or global interface loads without exceeding the design loads. So, it is often necessary to control and limit the input based on a load criterion. This means the test engineer should be able to assess the interface loads, even when load cannot be measured. This paper presents various approaches to evaluate interface loads using measured accelerations and by referring to mass operators. Various methods, from curve fitting techniques to finite element-based methods are presented. The methods are compared using signals with known imperfection to identify strengths and weaknesses of each mass operator definition.

Keywords: vibration; mass operator; acceleration measurement; load identification; neural network

1. Introduction

Spacecraft, their instruments and subcomponent are very often put through several vibration tests in order to verify their design and give confidence that they will survive the launch and any other critical in-orbit dynamic scenario. At component level, vibration tests are conducted with the aim to reach local or global interface loads without exceeding the design loads. Therefore, there is often a need to control and limit the input or notch based on a load criterion. However, despite having a load criterion, the interface load itself is rarely measured.

Indeed, to directly or indirectly measure the interface loads one would need to use, for example, load cells, strain gages or the shaker's coil current (ECSS-E-HB-32-26A 2013). These approaches present financial, programmatic and technical drawbacks. Load cells are costly, take space not taken into account in the design, and will often change the system's response so they need to be accounted for in all test prediction analyses. Strain gages require careful calibration to provide a robust indirect measurement of the interface loads. The coil current can only be used for the global interface load along the excitation direction and requires access to the coil current information and

*Corresponding author, Mechanical Engineer, Ph.D., E-mail: raymond.olympio@airbus.com

http://www.techno-press.org/?journal=aas&subpage=7 ISSN: 2287-528X (Print), 2287-5271 (Online)

good knowledge of the shaker dynamic behavior, especially when running through shaker's modes. Hence, loads are seldom measured and it is common practice to notch the input based on measured accelerations rather than loads. Unfortunately, this means that the test engineer conducts the test with no direct information about the interface load levels.
One way to check the interface load levels is to use a so called "mass operator" (MOP). The MOP is a mathematical tool used to derive loads from measured accelerations. Thus, no additional instrumentation is necessary. This requires however additional processing before and during the vibration test.

This paper first presents various approaches to derive interface loads from accelerations. Each method is implemented with Matlab® in the modular software Primodal® (Primodal 2015). Then, parametric studies are performed to understand the advantages and limitations of each method. This paper is a complement to (Olympio *et al.* 2016) where mass operators were applied to a different structure. More information about the implementation of the various mass operators are also available in (Olympio *et al.* 2016).

2. Theoretical background

Before performing a vibration test, it is common practice to calculate beforehand the expected structural response using the finite element method (FEM). Thus, it would be natural to use the corresponding finite element results to define a relationship between one quantity (e.g., loads, stresses, or strains) and accelerations at predefined locations on the structure and apply that same relationship to real measurements.

This assumes that the measurement points are well defined and the finite element model describes sufficiently well the structure's behavior. The validity of both assumptions is beyond the scope of this paper, and it is assumed in this paper that they are valid.

Using the linear FEM's formalism, the relationship between interface loads and acceleration can be written as

$$\{F(\omega)\} = \left([M] + \frac{1}{i\omega}[C] - \frac{1}{\omega^2}[K] \right) \{A(\omega)\} \tag{1}$$

Where:

- [K], [C] and [M] are the stiffness, damping and mass matrices respectively.
- {A} is the acceleration vector at given measurement points.
- {F} is the load vector containing the interface loads.

It can be noted that Eq. (1) may be rewritten to include other types of data (e.g. strain gage measurements, stress). For conciseness, this paper is only concerned with interface loads and accelerations.

The following sections describe different methods of deriving the relationships between interface loads and accelerations.

2.1 Sum of weighted accelerations

The classical MOP consists in finding a linear relationship between accelerations at given

points in the structure to loads (force or moment) at given (local or global) interfaces of the structure. This approach is also called sum of weighted accelerations (SWA) technique (Carne *et al.* 1992). For a single set of load and moment, it is expressed as in Eq. (2).

$$\begin{cases} F_{MOP}(\omega) = \sum_{i \in Sensors} m_i . A_i(\omega) = \{m\}^T . \{A\} \\ M_{MOP}(\omega) = \sum_{i \in Sensors} l_i . m_i . A_i(\omega) = \{m\}^T . [l] \{A\} \end{cases} \tag{2}$$

Where:

- A_i are acceleration measurements over the frequency range of interest.
- m_i are weighting coefficients.
- l_i is the lever arm between the acceleration point i and the interface point.

The m_i coefficients can be regarded as equivalent dynamic masses. Then Eq. (2) is nothing else than Newton's second law of motion for a rigid set of point masses. This means that stiffness and damping are not explicitly taken into account, rather this information are contained in $\{A\}$.

The existence and unicity of a set of weighting coefficients m_i that satisfies Eq. (2) is dependent on the choice of measurement locations. For example, in the case of redundant measurements, an infinite number of weighting coefficient sets exists. In the case of poorly defined measurement locations, some modes may not be observable so no acceptable solution exists.

2.1.1 Fitted SWA

The most straightforward method to calculate the weighting coefficients m_i of Eq. (2) consists in defining them as design variables of a minimization problem or curve fitting problem as in Eq. (3).

$$\begin{aligned} &\text{Minimize} \quad \frac{1}{2} \left\| F_{FEM}(\omega) - F_{MOP}(\omega) \right\|^2 \\ &\text{such that} \begin{cases} \sum_{i \in Sensors} m_i \le m_{system} \\ m_i > 0 \end{cases} \end{aligned} \tag{3}$$

Where:

- $F_{FEM}(\omega)$ is the vector of global or local interface loads calculated with the FEM.
- $F_{MOP}(\omega)$ is the vector of global or local interface loads calculated as the sum of weighted accelerations as in Eq. (2).

The constraints in Eq. (3) are physics-based constraints in that it is assumed that the weighting coefficients are equivalent masses. However, these constraints are not always valid for local interface loads, sensors oriented in a local coordinate system, etc. Therefore, although constraints help reduces the design space, they may also make it harder to find a satisfactory solution.

2.1.2 Max-flat procedure

Other SWA techniques have been developed in the early 1990s at Sandia National Laboratory and other institutions (Dobson *et al*. 1990, Carne *et al.* 1991, Carne *et al.* 1992). Some were applied for time signals to determine load during non-harmonic testing (e.g., shock test), other were developed for the frequency domain (Carne *et al*. 1992). One such method is briefly derived

here.

We are looking for frequency-independent parameters to estimate the interface loads from the accelerations. This means that the system's elastic energy is not taken into account and the [K] and [C] terms in Eq. (1) must be eliminated.

If $\{\Phi_k\}_{rigid}$ a rigid body mode vector of the structure, then $[K]\{\Phi_k\}_{rigid} = \{0\}$ and $[C]\{\Phi_k\}_{rigid} = \{0\}$. Therefore, let us assume that the acceleration vector is a linear combination of the rigid body modes

$$\{A(\omega)\} = \sum_i \{\Phi_i\}_{rigid} q(\omega) \tag{4}$$

Where $\{q(\omega)\}$ is the vector of the second derivatives of the modal coordinates. So, injecting Eq. (4) in Eq. (1) and pre-multiplying by $\{\Phi_k\}_{rigid}^T$ gives

$$\{\Phi_k\}_{rigid}^T \{F(\omega)\} = m_k . q_k(\omega) \tag{5}$$

Where $m_k = \{\Phi_k\}_{rigid}^T [M] \{\Phi_k\}_{rigid}$. We are actually looking for a relationship of the form

$$S(\omega) = \sum_{j \in Sensors} w_j . A_j(\omega) = \{w\}^T \{A(\omega)\} \tag{6}$$

Substituting Eq. (4) into Eq. (6)

$$S(\omega) = \{w\}^T . \left(\sum_i \{\Phi_i\}_{rigid} q_i(\omega) \right) = \sum_i \left(\{w\}^T . \{\Phi_i\}_{rigid} \right) q_i(\omega) \tag{7}$$

We can choose *w* such that

$$\{w\}^T . \{\Phi_i\}_{rigid} = \begin{cases} 1 & \text{if } i = r \\ 0 & \text{otherwise} \end{cases} \tag{8}$$

Then,

$$q_r(\omega) = S(\omega) = \{w\}^T \{A(\omega)\} \tag{9}$$

Finally, Eq. (5) becomes

$$\{\Phi_r\}_{rigid}^T \{F(\omega)\} = m_r . \{w\}^T \{A(\omega)\} \tag{10}$$

Thus, for a chosen rigid mode $\{\Phi_r\}_{rigid}$, one only needs to define $\{w\}$ that satisfies Eq. (8) to estimate the interface loads from Eq. (10).

The rigid modes can be extracted by performing a modal analysis with the known mass and stiffness matrices or by identification from the frequency response functions.

In general, there are less rigid modes than degrees of freedom so this problem is ill-conditioned. To improve the accuracy of the solution, it is necessary to have a well-conditioned

mode shape matrix. This can be achieved by including elastic modes in the mode shape matrix.

From the derivation, it is clear that this method is straightforward to apply using finite element modal data, but it has the following drawbacks:

- It is not well suited for local interface loads.
- It can only be used to estimate the loads for the first few modes.
- It cannot be applied to other types of measurements.

2.1.3 Frequency dependent SWA

It has been shown that the approach presented in 0 works well only over small frequency ranges with few modes (ECSS-E-HB-32-26A, 2013). The limitation over small frequency range or small number of modes of the fitted SWA can be addressed by defining frequency-dependent weighting coefficients.

Let $\omega_{i,0}<\omega_{i,1}<...<\omega_{i,N}$ be a subdivision of the frequency range of interest. Ideally, each subdivision contains at most one mode. Then the weighting coefficients are calculated over each domain as in Eq. (11).

$$\text{For K from 0 to N - 1}$$

$$\left|\begin{array}{l}\text{Minimize} \quad \frac{1}{2}\left\|F_{FEM}(\omega)-F_{MOP}(\omega)\right\|^2 \\ \text{such that} \quad \sum_{i\in Sensors} m_{i,K} \le m_{system} \\ \text{with} \quad \omega_{i,K} \le \omega < \omega_{i,K+1}\end{array}\right. \tag{11}$$

The results are also much improved compared because the fitting problem corresponding to the fitted SWA (Sec. 0) is divided into smaller and easier to solve fitting problems.

2.2 Artificial neural networks

Although more complex, artificial neural networks (ANN) present a more generalized approach to data fitting (Passino 2000). Thus, they appear promising to map directly and accurately interface loads to accelerations, or to calculate frequency-dependent weighting factors.

2.2.1 Direct load modeling

Before a test, an ANN (Fig. 1) would be trained using the FE data from any prediction analysis. Then, the trained ANN would be fed with acceleration measurements to give an estimate of the loads of interest during the test.

This straightforward approach presents one significant drawback. Training the ANN with unpolluted FE data can result in an over-specialized ANN: it maps perfectly the FE data but performs poorly when fed with a set of polluted accelerations (e.g., noisy signals).

One solution to this problem would be to train the neural network with data containing all known sources of uncertainties. The neural network would then perform better at predicting loads from contaminated signals. This approach would, in effect, consists in performing stochastic test predictions (ECSS-E-HB-32-26A 2013).

2.2.2 SWA approach

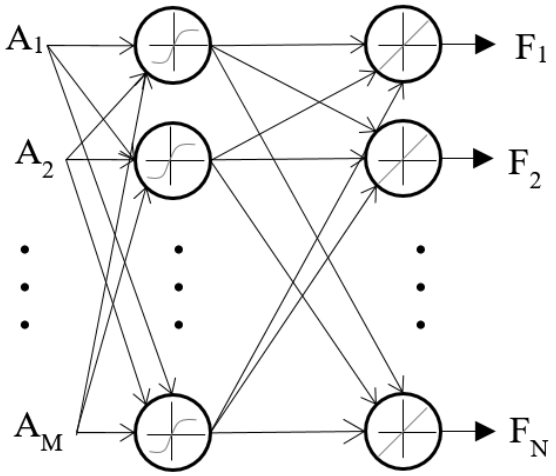

Fig. 1 ANN for the direct modeling of interface loads

ANN can also be used to model the weighting coefficients of Eq. (2). This is then a generalization of the frequency dependent SWA of Sec. 0. An example of such a neural network with one hidden layer is presented in Fig. 2. The neural network has one input, the frequency, and the outputs are the weighting coefficients m_1, m_2, … m_N of Eq. (2). The corresponding cost function is given in Eq. (12).

$$J = \frac{1}{2}\left\| F_{FEM}(\omega) - \sum_{i \in Sensors} m_i(\omega) A_i(\omega) \right\|^2 \tag{12}$$

A new neural network is created for each interface load. This helps reduce the size of the neural network and computational cost of training the neural network.

It can be noted that the fitted SWA of Sec. 0 corresponds to such an ANN with no hidden layer and only one neuron with a linear activation function in the output layer.

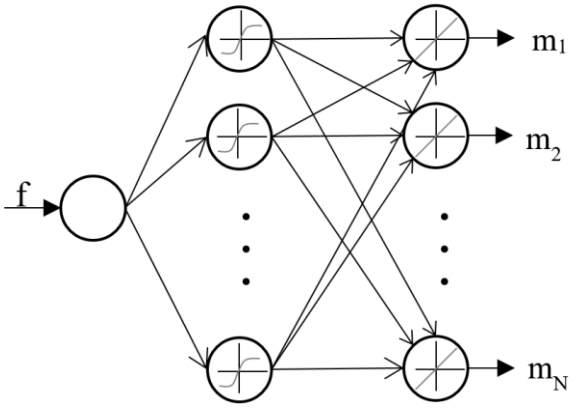

Fig. 2 ANN for the calculation of frequency dependent weights

For the results presented in this paper, the neurons' activation function is the radial basis function (Passino 2000) and the neural network has only one input: the frequency. One can consider adding more inputs to obtain mass coefficients dependent on other meaningful parameters (e.g., sweep rate, overall load level), but this is beyond the scope of this paper.

2.3 Super-element model

Eq. (1) is the equation solved by the FE solver when performing a vibration analysis. Therefore, the [K] and [M] matrices generated by the solver (e.g., MSC Nastran™) can be used directly. Taking the complete mass and stiffness matrix of a fully modeled structure is impractical. However, one can reduce these matrices using static reduction method (e.g., Guyan method) or dynamic reduction methods (e.g., Craig-Bampton method).

The matrices of in Eq. (1) can be obtained by performing a dynamic reduction of the FE model of the structure to be tested (Eq. (13)). The reduction method is performed with all the acceleration points defined as boundary nodes in order to have a well-conditioned problem.

$$\begin{Bmatrix} 0 \\ F_B \end{Bmatrix} = \left(\underbrace{\begin{bmatrix} [I] & [L_{mB}] \\ [L_{Bm}] & [M_{BB}] \end{bmatrix}}_{[\tilde{M}]} - \frac{i}{\omega}[\tilde{C}] - \frac{1}{\omega^2} \underbrace{\begin{bmatrix} [\Omega^2] & [0] \\ [0] & [K_{BB}] \end{bmatrix}}_{[\tilde{K}]} \right) \begin{Bmatrix} \eta \\ a_B \end{Bmatrix} \tag{13}$$

Where:

- Subscript *B* denotes entities at the boundary nodes.
- η represents the vector of generalized coordinates.
- a_B represents the vector of boundary accelerations.
- $[\Omega^2]$ is the matrix of eigenvalues.

The damping matrix $[\tilde{C}]$ is constructed assuming a modal damping. This allows easy tuning of the system's damping behavior based on measured damping.

With all the accelerations nodes defined as boundary nodes, the mass, damping and stiffness matrices of Eq. (2) are obtained by reducing $[\tilde{M}]$, $[\tilde{C}]$ and $[\tilde{K}]$ to the physical degrees of freedom used during the vibration test. The corresponding matrix $[T(\omega)]$ is the inverse of the FRF and the loads are obtained by simple matrix multiplication as in Eq. (14).

$$\{F_B\} = [T(\omega)]\{a_B\} \tag{14}$$

In a similar manner, the internal loads can be extracted from elements (e.g., springs) using the super-element's element force transformation matrix (MEF) reduced to the relevant degrees of freedom

$$\{F_I\} = -\frac{1}{\omega^2}[MEF(\omega)]\{a_B\} \tag{15}$$

With this method, one can tune the FE model by adjusting natural frequencies and damping to

match the measured responses. This is the clear advantage of this method over the SWA methods of Sec. 0 and Sec. 0 which cannot be adjusted based on measurements data without model update and new finite element analyses.

3. Evaluation

To evaluate the various MOP methods, an instrument and its supporting structure is considered. The MOP methods will be applied to calculate the global interface loads at the interface of the supporting structure and the local interface loads between the supporting structure and the instrument as illustrated in Fig. 3. In the rest of the paper, this instrument is assumed to be excited along the X-direction only.

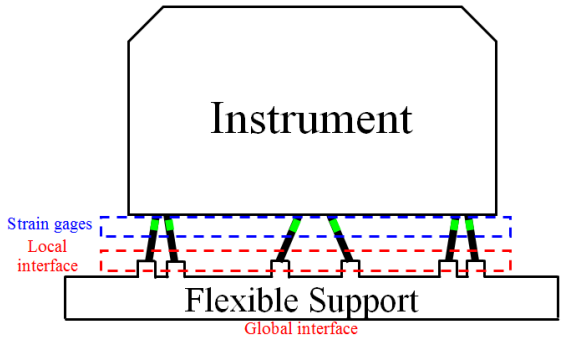

Fig. 3 Instrument and support

3.1 Baseline: Harmonic analysis

Table 1 lists the natural frequencies and effective masses of the baseline system in the 5-2000Hz frequency range. Figs. 5-7 illustrate the performance of the various MOP approached considered in this paper, for local and global interface loads. To evaluate the ability to model loads over large and small frequency ranges with numerous modes, the MOPs have been created with finite element data in the 5-2000 Hz and 5-500 Hz ranges.

Table 2 and Table 3 show the normalized root-mean-square deviation (NRMSD) between the baseline and the loads calculated with the MOPs considering the response up to 2000 Hz and up to 500 Hz respectively. The NRMSD is defined as in Eq (16). A value of 0 indicates perfect correlation with the baseline.

$$RMSD = \frac{1}{n}\sqrt{\sum_{1\le i\le n}\left(1-\frac{S_i^{MOP}}{S_i^{baseline}}\right)^2} \tag{16}$$

From the results, one can observe that the Max-Flat method estimate correctly only the first mode along the excitation direction (X). By definition it cannot be used to estimate local interface loads.

The other methods work very well over the entire frequency range. The ANN shows sharp peaks that could be eliminated by additional training.

Table 1 Natural frequencies and modal effective mass fraction from the original FE model

Sum		38.06%	38.69%	37.29%	39.70%	39.94%	44.34%
Mode No.	Freq [Hz]	Modal effective masses fraction					
		Tx [%]	Ty [%]	Tz [%]	Rx [%]	Ry [%]	Rz [%]
1	74.90	9.30%	0.11%	4.76%	0.39%	14.78%	0.54%
2	197.19	0.91%	12.65%	16.30%	9.80%	0.22%	9.68%
3	316.19	7.75%	0.36%	7.74%	1.12%	12.43%	0.44%
4	468.00	13.12%	0.64%	0.64%	0.37%	9.77%	0.05%
5	644.84	3.78%	21.55%	6.03%	24.26%	1.02%	28.88%
6	727.49	1.14%	2.67%	1.58%	3.27%	0.35%	4.65%
7	836.33	1.96%	0.56%	0.25%	0.37%	1.32%	0.04%
8	926.17	0.09%	0.16%	0.00%	0.13%	0.06%	0.06%

Table 2 Correlation table considering the response up to 2000Hz

	Internal Fx	Internal Fy	Internal Fz	Global Fx	Global Fy	Global Fz
SWA	0.72%	0.53%	0.34%	0.33%	0.28%	0.46%
Max-Flat	5.60%	5.60%	5.60%	3.87%	8.38%	26.81%
WNN	0.71%	0.59%	0.49%	0.13%	0.12%	0.84%
SE	0.68%	0.21%	0.42%	0.11%	0.25%	1.14%
ANN	8.38%	2.88%	1.03%	0.42%	0.78%	4.47%

Table 3 Correlation table considering the response up to 500Hz

	Internal Fx	Internal Fy	Internal Fz	Global Fx	Global Fy	Global Fz
SWA	0.55%	0.50%	0.35%	0.11%	0.11%	0.30%
Max-Flat	5.53%	5.53%	5.53%	3.38%	5.89%	10.96%
WNN	0.31%	1.37%	0.84%	0.08%	0.04%	0.25%
SE	0.73%	0.23%	0.47%	0.27%	0.15%	0.36%
ANN	1.19%	0.79%	0.22%	0.12%	0.28%	1.01%

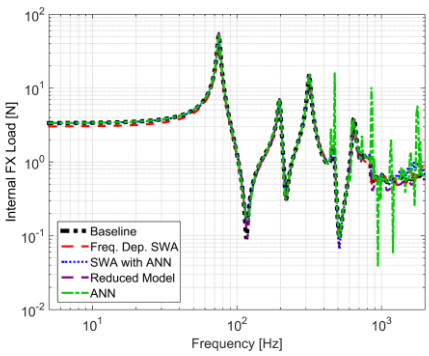

(a)

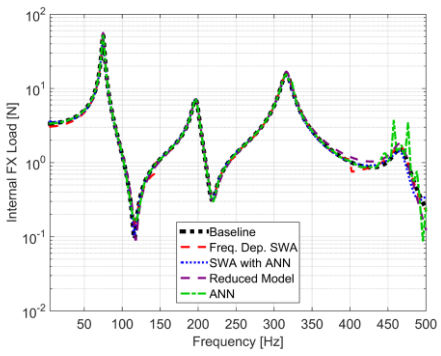

(b)

Fig. 4 Baseline-Local interface loads considering the (a), (c), (e) the 5-2000 Hz range and (b), (d), (f) the 5-500 Hz range

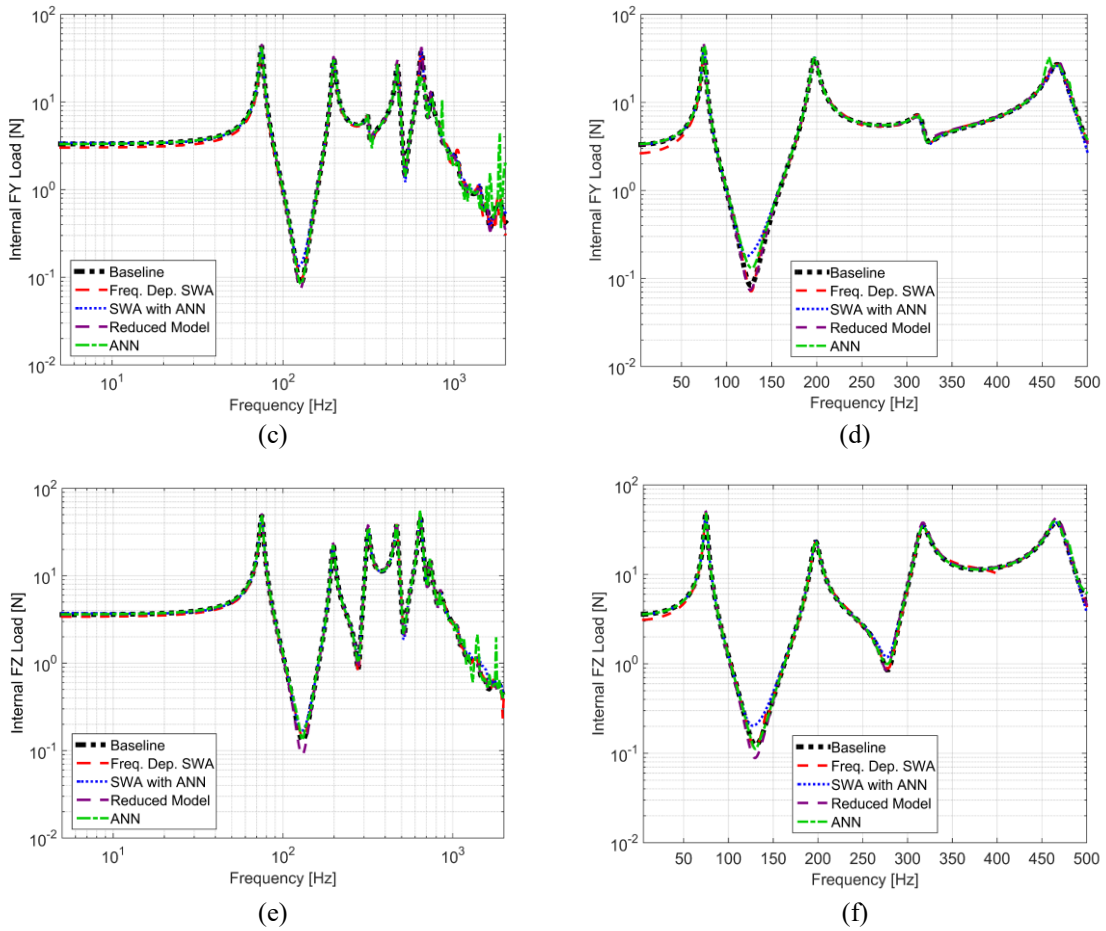

Fig. 5 Continued

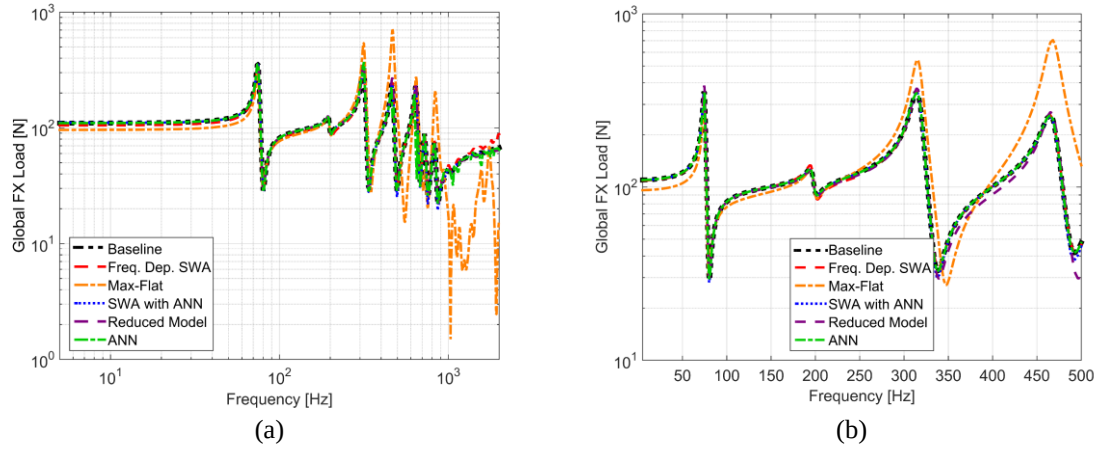

Fig. 6 Baseline-Global interface loads calculated with each MOP considering (a), (c), (e) the 5-2000 Hz range and (b), (d), (f) the 5-500 Hz range

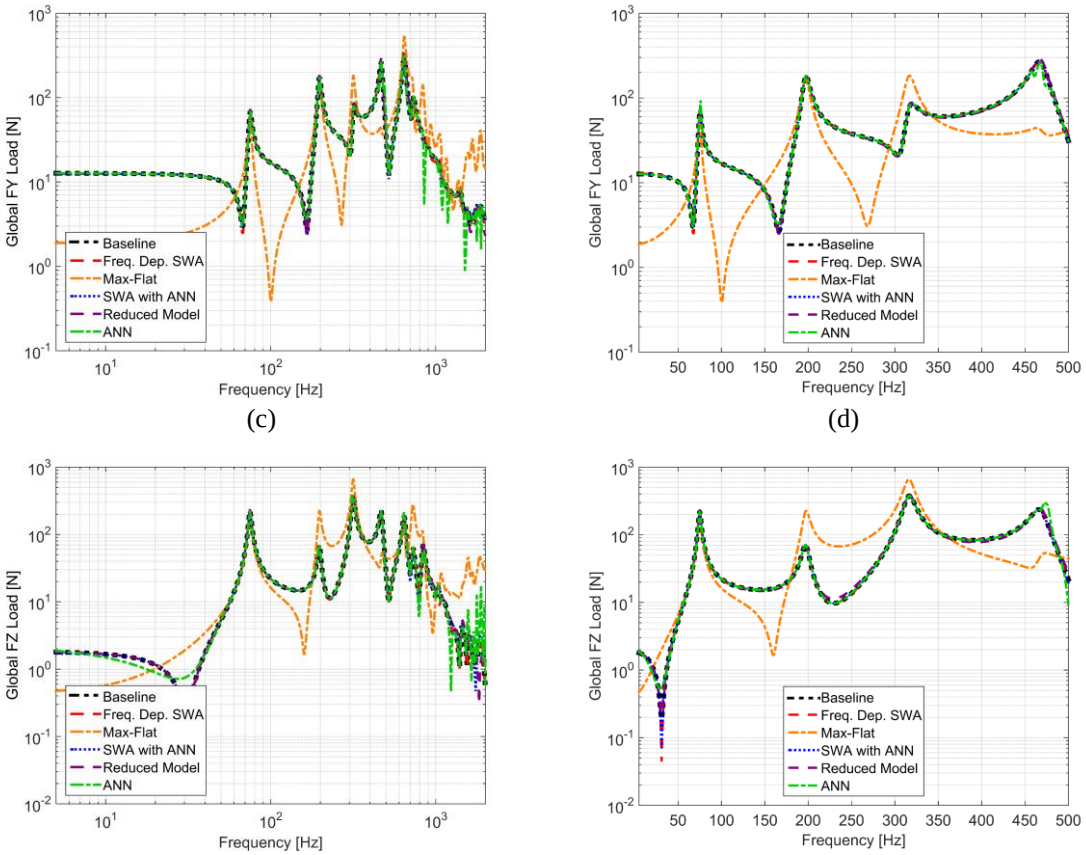

Fig. 7 Continued

3.2 Parametric studies

To evaluate the proposed MOPs, baseline accelerations and interface loads were calculated with the FEM. Then the baseline data (Sec. 0) was corrupted by adding frequency shifts, damping, sensor orientation errors or noise, and the MOP were tested with these corrupted inputs. This allows testing the MOPs with complete control on the source of error. The MOP (e.g., weighting factors, neural network definition, super-element's matrices) are not changed in the following parametric studies.

One could also consider evaluating a method when one measurement channel is missing. In this situation, it is always better to recalculate the MOP. This task can be considered effortless with a fully automated mass operator tool as done in *Primodal* as part of this study.

3.2.1 Modeling uncertainty

Stiffness

To evaluate the effect of frequency shifts, the material definitions in FE model were modified to generate some shift in modal frequencies, the mode order is unchanged. The first 8 natural frequencies and effective masses of the modified structure are listed in Table 4 and can be compared to those of the baseline structure (Table 1).

Table 4 Natural frequencies and modal effective mass fraction from the modified FE model

Sum		38.16%	38.84%	37.29%	39.84%	40.03%	44.49%
Mode No.	Freq. [Hz]	Modal effective masses fraction					
		Tx [%]	Ty [%]	Tz [%]	Rx [%]	Ry [%]	Rz [%]
1	70.19	9.39%	0.09%	4.97%	0.37%	15.01%	0.58%
2	188.12	0.91%	13.07%	16.13%	10.18%	0.21%	10.08%
3	300.38	7.57%	0.38%	7.60%	1.16%	12.14%	0.40%
4	455.85	13.68%	0.54%	0.66%	0.29%	10.20%	0.10%
5	607.10	4.20%	23.28%	6.92%	26.32%	1.10%	31.57%
6	714.26	0.54%	0.91%	0.84%	1.18%	0.15%	1.83%
7	827.23	1.89%	0.58%	0.26%	0.38%	1.25%	0.05%
8	924.38	0.08%	0.15%	0.00%	0.12%	0.06%	0.06%

Fig. 8 shows the performance of each MOP methods with respect to frequency shift between the exact interface load and the MOP-derived interface loads. Table 5 provides the NRMSD between the baseline and the MOP derived loads.

Table 5 Correlation table with incorrect material properties

	Internal Fx	Internal Fy	Internal Fz	Global Fx	Global Fy	Global Fz
SWA	10.99%	1.91%	2.62%	0.22%	0.39%	1.03%
Max-Flat	5.49%	5.49%	5.49%	3.21%	5.86%	10.76%
WNN	6.27%	8.51%	3.99%	0.47%	0.36%	0.83%
SE	2.05%	2.38%	1.44%	2.33%	131.57%	27.14%
ANN	16.31%	1.92%	1.87%	0.39%	0.83%	1.71%

All the MOPs perform well at identifying the peak responses. However, the reduced model and Max-Flat methods perform poorly at estimating the peak responses' amplitude. This can be expected because these methods are derived with the structural matrices. The SWA methods and ANN perform well at estimating the first 3 modes' peaks and match closely the expected loads (baseline of the modified model). From these results, none of the MOP can fit the expected response beyond the 3rd mode.

Damping

To evaluate the effect of damping difference, the baseline harmonic analysis was re-performed with a Q factor of 50 instead of 25.

Fig. 9 shows the performance of each MOP methods with respect to damping difference

between the exact interface load and the MOP-derived interface loads. Table 6 provides the NRMSD between the baseline and the MOP derived loads.

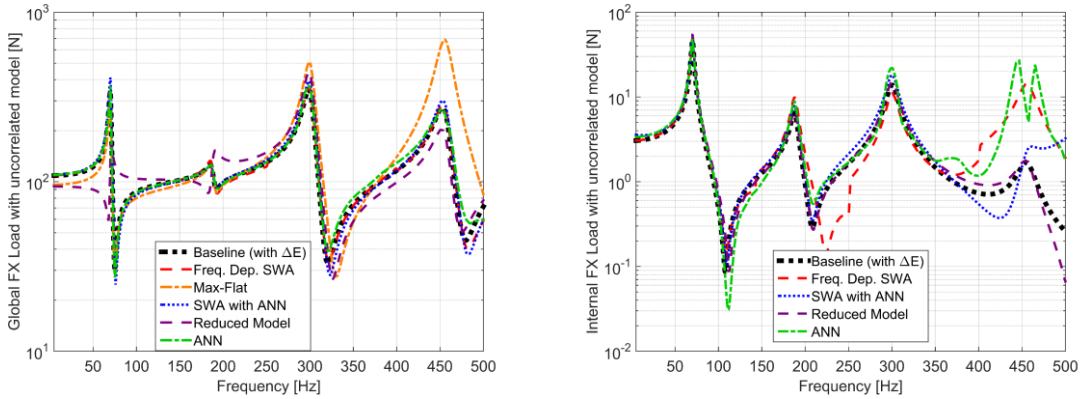

(a) (b)

Fig. 8 Effect of frequency shift in the input data on the MOP's load estimation of (a) Global interface loads and (b) local interface loads

Table 6 Correlation table with incorrect damping

	Internal Fx	Internal Fy	Internal Fz	Global Fx	Global Fy	Global Fz
SWA	0.47%	0.53%	0.39%	0.13%	0.09%	0.23%
Max-Flat	5.49%	5.49%	5.49%	5.41%	8.69%	12.53%
WNN	0.24%	0.44%	0.29%	0.06%	0.03%	0.19%
SE	0.97%	0.27%	0.51%	0.35%	1.07%	2.30%
ANN	19.48%	2.42%	1.22%	1.58%	1.47%	2.00%

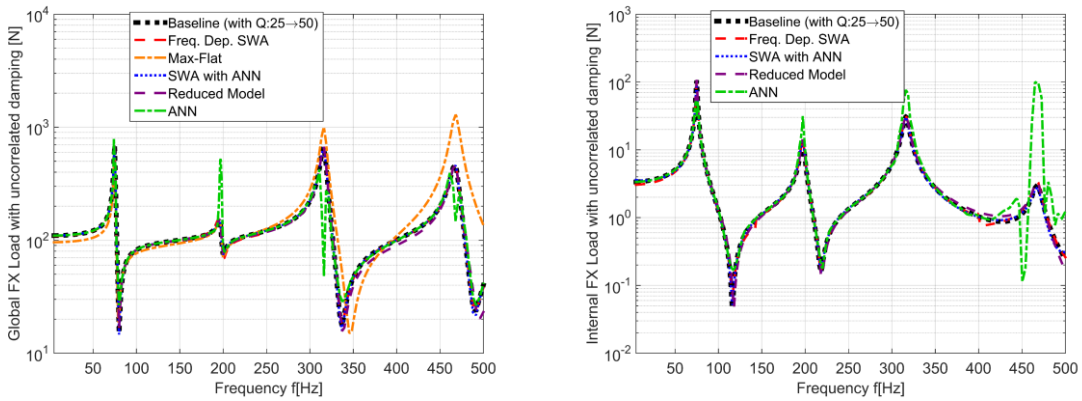

(a) (b)

Fig. 9 Effect of damping difference in the input data on the MOP's load estimation

Except for the ANN method, all the methods perform well and match closely the expected loads (baseline of the modified model). This is to be expected for the SWA methods because the

damping information is contained in the acceleration measurements.

The ANN match well up to the exact peak location where the estimated amplitude is off by up

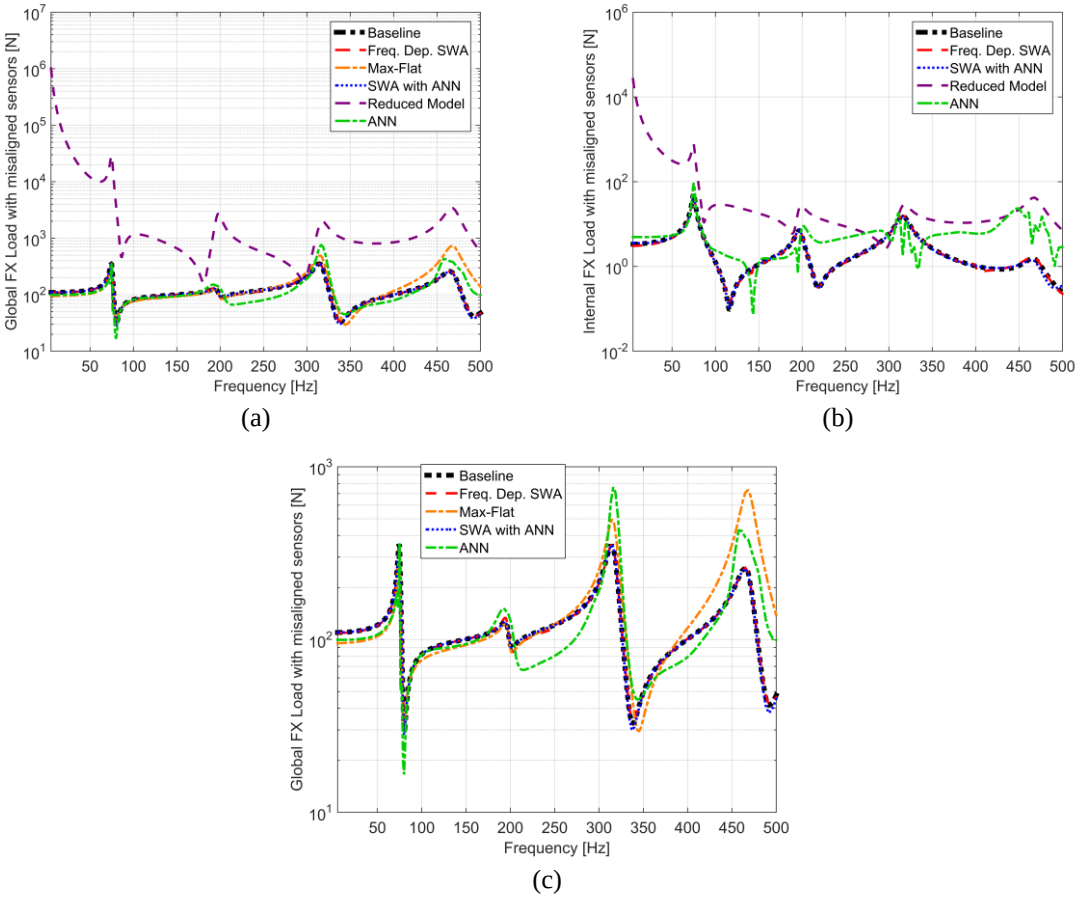

Fig. 10 Effect of uncorrected orientation error in the input data on the MOP's load estimation

Table 7 Correlation table with sensor orientation error

	Internal Fx	Internal Fy	Internal Fz	Global Fx	Global Fy	Global Fz
SWA	0.55%	0.50%	0.35%	0.11%	0.11%	0.30%
Max-Flat	5.53%	5.53%	5.53%	3.47%	5.75%	12.54%
WNN	0.31%	1.37%	0.84%	0.08%	0.04%	0.25%
SE	2657.70%	4289.49%	753.93%	3118.76%	12169.52%	686696.50%
ANN	27.49%	13.15%	3.41%	2.07%	9.07%	37.93%

to one order of magnitude. This is expected because the relationship between sensors' amplitude values at various frequencies learned by the ANN is no longer valid.

3.2.2 Sensor orientation uncertainty

Another source of uncertainty is the sensor orientation errors. Although this can be corrected

with sufficient test data, it is important to understand how they affect the loads estimated with a MOP. A random orientation uncertainty along all sensor axis and comprised between -10 deg and 10 deg was added to the acceleration data and fed to each MOP.

Fig. 10 shows the performance of each MOP methods with respect to sensor orientation error. Table 7 provides the NRMSD between the baseline and the MOP derived loads.

The SWA and Max-Flat methods can correctly estimate the location and shape of the resonance peaks. The predictions with these MOPs result in an error on the amplitude over the entire frequency range. Thus, when this amplitude error is detected, it can be corrected in a direct manner.

On the other hand, the ANN and the reduced model can't be used to correctly estimate the interface loads. Indeed, load estimation with the ANN or reduced model shows unrealistic load at low frequency or the large oscillations even outside resonances.

3.2.3 Noise

The last source of error considered in this paper is the measurement noise. This usually cannot be controlled or easily improved. Fig. Fig. 11 shows the effect of noise (signal-to-noise ratio, SNR=20) on the MOP-calculated interface loads. Fig. Fig. 12 shows the effect of filtered noise on the loads estimated using the super-element model and the ANN. Table 8 provides the NRMSD between the baseline and the MOP derived loads for the unfiltered and filtered signals.

Table 8 Correlation table with white Gaussian noise (SNR=20)

	Internal Fx	Internal Fy	Internal Fz	Global Fx	Global Fy	Global Fz
SWA	84.29%	343.73%	407.32%	0.47%	19.46%	49.12%
Max-Flat	5.53%	5.53%	5.53%	3.32%	6.33%	45.21%
WNN	0.54%	1.60%	0.92%	0.15%	0.10%	0.20%
SE	3276.94%	7411.28%	6116.68%	3182.66%	86191.11%	890591.56%
NN	16.84%	19.20%	23.52%	0.97%	5.96%	164.71%
SE (filtered)	0.90%	0.76%	0.68%	0.42%	0.44%	1.49%
NN (filtered)	2.71%	0.89%	4.79%	0.28%	1.06%	6.07%

For global loads in the excitation direction, all the methods, except for the super-reduced model approach, perform well with moderate noise. Indeed, for SWA based approaches, the effect of noise is proportional to the highest mass coefficients. So in general, the effect of noise on the load in the excitation direction remain smalls.

This is not true for cross-axis loads as seen in Table 8, because for cross axis responses, which are generally low amplitude responses, are more sensitive to noise. Further, the importance of cross axis responses is greater when estimated cross axis loads, as opposed to loads in the excitation direction.

With the super-element model, any small relative difference between measurements points leads to an increase in load levels proportional to the structural stiffness. So, the elastic loads are orders of magnitude higher than inertial load, especially, in the quasi-static frequency range where elastic loads should theoretically be negligible. This leads to artificial elastic loads in the equilibrium equation and overestimation of the interface loads.

The neural network approach is affected by noise, but it is still able to predict major peaks in the loading direction. The poor performance of the ANN can be attributed to incomplete training. Better training (e.g., adding noisy data in the training samples) could make the neural network even less sensitive to noise.

To alleviate the problem of noise, a filter has been applied to the corrupted acceleration signals. As shown in Fig. 12, the load estimation by the reduced model is significantly improved. In this example, as well as in other trials (Olympio *et al.* 2016), the implemented filter appears to work well and the actual load can be retrieved.

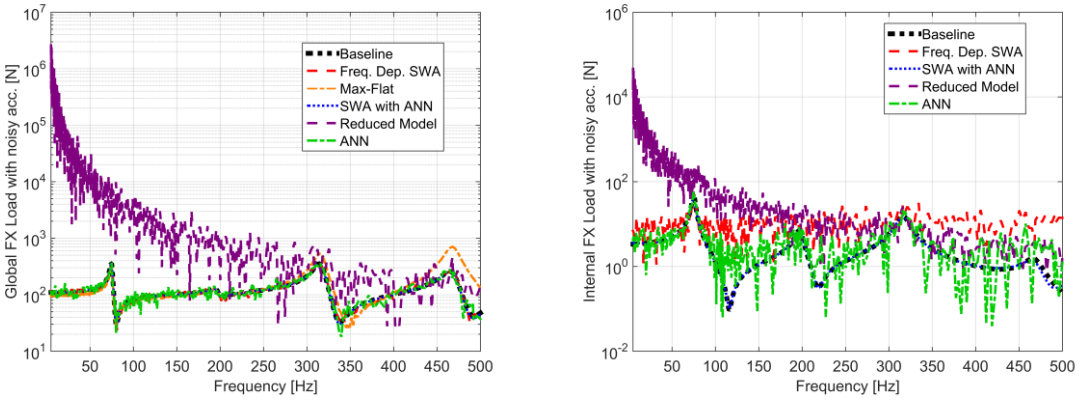

(a) (b)

Fig. 11 Effect of noise (SNR=20) in the input data on the MOP's load estimation

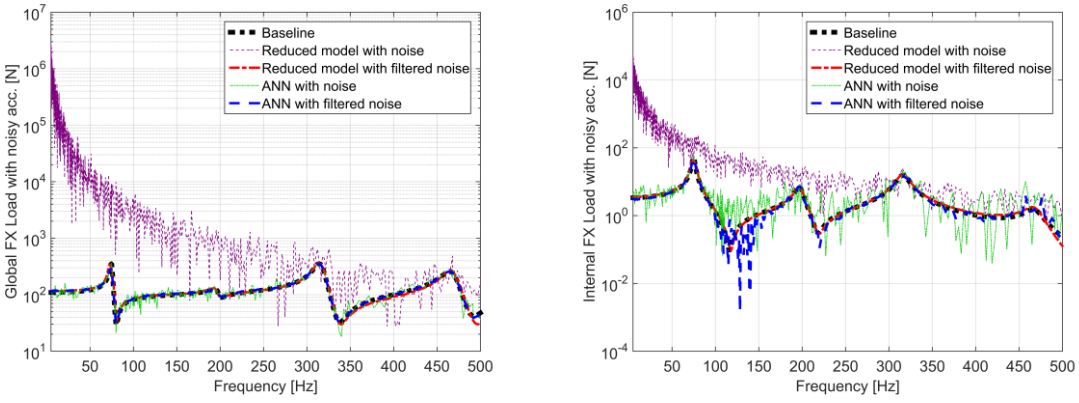

(a) (b)

Fig. 12 Filtering of noisy (SNR=20) acceleration signals

4. Conclusions

From the users' point of view, the ideal mass operator should be easy to use and robust with respect to modeling error, noise and instrumentation set up. Also, it should be capable of

estimating loads over a wide frequency range to apply it for both sine and random vibrations of spacecraft and their instruments. To answer these requirements, several approaches to deriving a

Table 9 Advantage and limitations of the mass operator approaches

	Easy creation/ update	Valid over large frequency ranges	Robust to noise	Robust to sensor dir	Robust to modeling error	Versatile	Wide frequency range	Fast utilization	No Optimization	Can be tuned in-line	Comments
Fitted SWA	•		•	•	•	•		•			Only valid over a couple of modes at best.
Max-Flat	•		•		•			•	•	•	
Frequency-dependent SWA	•	•	•	•	•	•	•	•			
Neural Network with SWA		•	•	•	•	•	•	•			• Proper training can be challenging.
Neural Network		•				•	•	•			• Known uncertainties can be included.
Super-element model		•					•		•	•	• Slow due to multiple matrix operations with dense matrices. • Natural frequencies and damping can be updated with minimal effort.

mass operator have been presented and a tool has been implemented in MATLAB® as a new module for Primodal®.

To estimate the performance of the mass operators with imperfect accelerations measurements, FE-based data were modified and fed to various mass operators. This allowed making several observations regarding the robustness of the mass operators. The main advantages and drawbacks are listed in Table 9.

Two major issues in the practical use of mass operators were identified: the impact of the inaccurate sensor orientation and the signal noise. No solution was investigated for the former. A solution would be to correct the measurements using, for example, the measurements in the quasi-static range, based on test along multiple excitation directions, as implemented in Primodal®'s SENSOR module.

It was also shown that the effect of white Gaussian normal noise can be reduced with an appropriate filtering technique. Additional work is necessary to show or propose filters that work in a majority of practical cases, and to overcome the issues related to the sensor orientation.

Although, the behavior of the mass operators was mainly examined in the frame of sine excitation, load evaluation under random excitation is also possible as shown with the validity of

some MOP up to 2000 Hz. Further verification of the tool via parametric studies and improvements of the tool are foreseen in the near future. The capability of the tool to estimate other type of data (e.g., stresses) based on measured accelerations is under study.

Acknowledgments

This study was funded by the Airbus Defence and Space's TSOMM-Industrial innovation.

References

Allemang, R.J. and Brown, D.L. (2006), "A complete review of the complex mode indicator function (CMIF) with applications", *Proceedings of the International Conference on Noise and Vibration Engineering*, Katholieke Universiteit Leuven, Belgium.

Boudraa, A.O., Cexus, J.C. and Saidi, Z. (2004), "EMD-based signal noise reduction", *J. Sign. Proc.*, **1**(1), 33-37.

Carne, T.G., Bateman, V.I. and Dohrmann, C.R. (1991), "Force reconstruction using the inverse of the mode-shape matrix", *Proceedings of the 13th Biennial ASME Vibration Conference*, Miami, Florida, U.S.A.

Carne, T.G., Bateman, V.I. and Mayes, R.L. (1992), "Force reconstruction using a sum of weighted accelerations technique-max-flat procedure", *Proceedings of the 10th International Modal Analysis Conference*.

Dobson, B.J. and Rider, E. (1990), "A review of the indirect calculation of excitation forces from measured structural response data", *Proceedings of the Institution of Mechanical Engineers, Part C: Journal of Mechanical Engineering Science*, **204**(2), 69-75.

ECSS-E-HB-32-26A (2013), *Space Engineering: Spacecraft Mechanical Loads Analysis Handbook*.

Olympio, K.R., Blender, F., Holz, M., Kommer, A. and Vetter, R. (2016), "Implementation and test of a robust mass operator tool", *Proceedings of the 14th European Conference on Spacecraft Structures, Material and Environmental Testing*, Toulouse, September.

Passino, K.M. (2005), *Biomimicry for Optimization, Adaptation, and Decision-Making in Computer Control and Automation*, Springer Science & Business Media, London, U.K.

Primodal User's Manual (2015), *Version 2.8*.

CC